Physics – Uspekhi **65** (3) 215 – 226 (2022)

REVIEWS OF TOPICAL PROBLEMS PACS numbers: **75.10. – b**, **75.30. – m**, 75.40.Cx, 75.50.Ee

Microscopic approach to the description of spin torques in two-dimensional Rashba ferromagnets and antiferromagnets

A A Pervishko, D I Yudin

DOI: https://doi.org/10.3367/UFNe.2021.04.038964

Contents

1. Introduction **215**
2. Microscopic approach. Calculating the response function **216**
3. Two-dimensional Rashba ferromagnet **218**
3.1 Dzyaloshinskii–Moriya interaction; 3.2 Spin-orbit torques; 3.3 Spin-transfer torques
4. Two-dimensional Rashba antiferromagnet **221**
4.1 Hamiltonian of the Rashba antiferromagnet; 4.2 Spin-orbit torques; 4.3 Antiferromagnetic switching; 4.4 Gilbert damping
5. Conclusion **225**
References **226**

Abstract. We review the most significant results obtained in the framework of the microscopic approach to a systematic study of magnetic dynamics in two-dimensional ferromagnetic and antiferromagnetic materials with a strong Rashba spin-orbit coupling. For model systems, we discuss the microscopic derivation of the Gilbert damping tensor, spin-orbit and spin-transfer torques, and symmetric and antisymmetric exchange interactions. It is shown that in both antiferromagnetic and ferromagnetic systems, the presence of a sufficiently strong spin-orbit coupling leads to an anisotropy of spin torques and Gilbert damping. We focus on an analysis of spin-orbit torques in a two-dimensional Rashba antiferromagnet. We also address the possibility of switching the antiferromagnetic order parameter via short current pulses in the plane of the sample.

Keywords: ferromagnet, antiferromagnet, spin-orbit coupling, Dzyaloshinskii–Moriya interaction, spin-transfer torque, spin-orbit torque, Gilbert damping

1. Introduction

Significant technological advances seen in recent decades in information processing and storage systems have largely been to a systematic study of collinear magnetic materials. The pioneering work of Grünberg [1] and Fert [2] on giant magnetoresistance, carried out in the 1980s and awarded the Nobel Prize in 2007 [3, 4], laid the foundations for the research area currently known as spintronics. Subsequent studies of the dynamics of ferromagnetic systems led to the discovery of magnetization switching effected by an external spin-polarized current in a sample, a possibility first noted by Slonczewski [5] and Berger [6]. Physically, this process can be explained by the appearance of a spin-transfer torque (STT) in a magnetic system due to the spin current, which mainly originates in the spin Hall effect, as is discussed in detail, for example, in [7].

In turn, the experimental detection of the spin Hall effect associated with the buildup of spin polarization at the sample boundaries by optical and electrical methods is an actively developing area of research [8]. If the ferromagnetic material is a dielectric, energy and information are transferred by the magnon current [9, 10]. At the same time, in ferromagnetic systems without inversion symmetry it is possible to stabilize the nontrivial particle-like textures in form of skyrmion [11–13].

From the standpoint of technological applications, the main interest for spintronics has been attracted to the study of ferromagnets [14–17], largely due to the possibility to control their magnetic properties via external electric current or optical pulses [18–21], while antiferromagnetic materials, which are much more common in nature, remained terra incognita because the antiferromagnetic order parameter could not be affected by any external perturbations [22, 23].

Research that spanned over many years revealed a number of essential shortcomings in the practical use of ferromagnetic materials. A relatively high magnitude of switching currents and hence significant heat generation and energy losses, together with the slowness of the switching itself, make the device operation unstable. The use of tunnel currents perpendicular to the plane (CPP) of the structure [24, 25] allowed increasing the switching rate, but required an even higher switching voltage, inevitably resulting in a much higher heating of the structure. Magnetic switching in ferromagnetic materials via tunneling in-plane currents (CIP) (in the plane of the structure) [26, 27], in turn, significantly reduces the switching current while making the proposed devices too slow. These shortcomings are exacerbated by a

A A Pervishko (†), **D I Yudin** (*)
Skolkovo Institute of Science and Technology, Bol'shoi bul'var 30, 121205 Skolkovo, Moscow, Russian Federation
E-mail: (†) a.pervishko@skoltech.ru, (*) d.yudin@skoltech.ru

Received 14 November 2020, revised 7 April 2021
Uspekhi Fizicheskikh Nauk **192** (3) 233 – 246 (2022)
Translated by S Alekseev

lack of ferromagnetic materials that can be easily integrated into the existing technological processes in the semiconductor industry.

Currently, the research focus has shifted toward the study of materials with extremely low magnetization, such as antiferromagnets, in which the magnetic field is compensated on atomic scales (see, e.g., review [28]). The fundamental possibility of using antiferromagnetic materials in spintronics was first demonstrated for a system made of an antiferromagnetic metal and a ferromagnet separated by a dielectric layer [29, 30]. Such a heterostructure has an anisotropic magnetoresistance, which is explained by a relatively strong spin-orbit coupling. Subsequently, the use of CuMnAs was proposed [31], in which antiferromagnetic domains can be switched using ultrashort laser pulses [28], opening up the way to designing antiferromagnetic magnetoresistive memory, whose prototypes have already been demonstrated [32, 33]. These experiments are widely regarded as a breakthrough into a new field of terahertz spintronics, where the microscopic switching mechanism is introduced by so-called spin-orbit torques (SOTs), which are by definition linear in the components of the electric field vector [34].

Undeniable advantages of antiferromagnets include their insensitivity to external magnetic fields, the absence of demagnetization fields, and much shorter spin switching times. It should be noted that the antiferromagnetic resonance frequency is several orders of magnitude higher than a similar parameter of ferromagnetic systems, that provides the possibility to switch from the gigahertz range to the terahertz range in antiferromagnetic spintronics devices.

Fully electrical switching of magnetic domains turns out to be most efficient in systems with sufficiently strong spin-orbit coupling, which provides an effective mechanism that couples the electronic and magnetic degrees of freedom [35, 36]. In quasi-two-dimensional bilayers of conducting and magnetic materials, the spin-orbit torque induced by an external electric current can be used to move domain walls or switch the magnetic orientation [37]. In the absence of spin-orbit coupling, spin torques arise only in systems with a nonuniform magnetization profile, so-called spin-transfer torques [15, 38], which, according to the conventional classification, are linear in the components of the electric field vector and in the first spatial derivatives of the magnetization vector. It is interesting to note that, due to the presence of a strong spin-orbit coupling, spin torques can also appear in structures containing a magnetic topological insulator. However, the influence of a magnetic material brought into contact with a three-dimensional topological insulator on the properties of surface states of the topological insulator requires a more detailed study, as does the problem of the influence of bulk effects of the topological insulator on the spin torques (see review [34]).

Despite the scientific community's considerable interest in the problems of spin dynamics in ferromagnetic and antiferromagnetic materials in the presence of a strong spin-orbit coupling, their theoretical description remains largely phenomenological. This approach is typically limited to the Landau–Lifshitz–Gilbert equations with arbitrarily chosen terms [39, 40] to describe the effect of spin-orbit and spin-transfer torques on the magnetization or the Néel vector.

For a typical heterostructure consisting of ferromagnet and metal layers with strong spin-orbit coupling, the number of different spin-orbit and spin-transfer torques is determined by the symmetry of the system [41]. In the phenomenological description, all these terms enter the equation with unknown coefficients; moreover, in two-dimensional systems, they are typically unknown functions of the magnetization vector components. This strongly limits the applicability of the phenomenological approach for complex-symmetry systems, such as layered systems with strong spin-orbit coupling, which are of primary importance in technological applications. The much faster dynamics of the Néel vector than that of the magnetization vector in a ferromagnet also makes the nonadiabatic contributions to the spin torques fundamentally important, and hence the number of unknown parameters in the phenomenological theory is at least doubled.

We note that the use of layered antiferromagnetic semiconductors leads to additional difficulties in describing the system because of the nontrivial and generally anisotropic band structure. These and many other problems with the phenomenological approach can be resolved within the microscopic theory.

In this review, we consider the major theoretical results obtained in the framework of a microscopic analysis of two-dimensional collinear magnetic systems with strong spin-orbit coupling, with the s–d exchange character of the interaction between a localized magnetic moment and conduction electrons taken into account [37, 42–55].

In Section 2, we address the microscopic approach for the description of magnetic systems in general terms. Within the local mean-field approximation in the continuum limit, we write a generalized Kubo–Streda formula for the spin torque tensor, connecting the local nonequilibrium spin polarization of conduction electrons with the electric field and the gradient and time derivative of the magnetic order parameter.

In Sections 3 and 4, the microscopic techniques that we discuss are used to analyze model two-dimensional ferromagnets and antiferromagnets with a strong Rashba spin-orbit coupling in the constant-field and Gaussian-disorder approximation; we address the contribution of conduction electrons to the Gilbert damping and its anisotropy and estimate the strength of symmetric and antisymmetric (Dzyaloshinskii–Moriya) exchange interactions. The results presented in Section 3 for the Rashba model of a two-dimensional ferromagnet clearly demonstrate a significant anisotropy of spin torques for systems with a strong spin-orbit coupling. In Section 4, we review the results for a model antiferromagnet with a strong Rashba spin-orbit coupling in the metallic and semimetallic regimes and also show that, just as in two-dimensional ferromagnets, strong spin-orbit coupling leads to a significant anisotropy of spin torques and Gilbert damping.

2. Microscopic approach. Calculating the response function

To describe two-dimensional magnetic systems within a microscopic approach, we consider the s–d model of a two-dimensional magnet with one (ferromagnetic system) or two (antiferromagnetic system) sublattices and with the local exchange interaction between localized magnetic moments $\mathbf{S}_i$ and itinerant electrons, whose contribution to the Hamiltonian is

$$H_{\mathrm{sd}} = -J_{\mathrm{sd}} \sum_i (\mathbf{S}_i\, \boldsymbol{\sigma})_{\sigma\sigma'}\, c^{\dagger}_{i\sigma} c_{i\sigma'}\,, \tag{1}$$

where $c_{i\sigma}$ and $c_{i\sigma}^{\dagger}$ are the annihilation and creation operators of an electron with spin projection σ at the ith lattice site, the components of the vector $\boldsymbol{\sigma} = (\sigma_x, \sigma_y, \sigma_z)$ are the Pauli matrices acting on the spin index of conduction electrons, and J_{sd} is the s–d exchange coupling constant. From term (1), the evolution of a localized magnetic moment is described by the equation

$$\frac{\partial \mathbf{S}_i}{\partial t} = \frac{J_{\mathrm{sd}}}{\hbar}\,\mathbf{S}_i \times \mathbf{s}_i\,, \tag{2}$$

where $\mathbf{s}_i = \langle c_{i\sigma}^{\dagger}\boldsymbol{\sigma}_{\sigma\sigma'}c_{i\sigma'}\rangle$ and the angular brackets denote averaging over the ground state of the Hamiltonian of itinerant electrons. In the continuum limit, the local magnetic moments and the spin densities of conduction electrons are assumed to change insignificantly on atomic scales, which allows representing them as $\mathbf{s}(\mathbf{r}) = \mathcal{A}^{-1}\sum_i \mathbf{s}_i$, where $\mathcal{A}$ is the area of a unit cell.

For simplicity of subsequent discussion, we restrict ourself to considering a single-domain magnetic material, meaning that, in the case of a ferromagnet, we assume all spins to be oriented the same direction and their absolute values to be equal, $\mathbf{S}_i = \mathbf{S}$; in the case of an antiferromagnet with two sublattices A and B, we assume that the spins at neighboring sites are opposite, $\mathbf{S}^{\mathrm{A}} = -\mathbf{S}^{\mathrm{B}} = \mathbf{S}$. Under the assumption that $|\mathbf{S}| = S \gg 1$, the quantity $\Delta_{\mathrm{sd}} = |J_{\mathrm{sd}}|S$ determines the energy scale of the s–d interaction. The dynamics of localized magnetic moments is typically much slower than that of conduction electrons, which allows describing the magnetic subsystem in terms of a classical vector field $\mathbf{m}(\mathbf{r}) = \mathbf{S}/S$.

In the mean-field approximation, the nonequilibrium spin polarization of conduction electrons $\mathbf{s}(\mathbf{r}, t)$ arises as a response to a change in both the classical field $\mathbf{m}(\mathbf{r}, t)$ (here and hereafter, $\mathbf{m}(\mathbf{r}, t)$ represents the magnetization of a ferromagnet or each sublattice of an antiferromagnet) and the external electric field $\mathbf{E}(t)$ and is in general strongly nonlocal in space and time. But, under the assumption that the magnetization of a ferromagnet (or of each sublattice of an antiferromagnet) and the electric field strength are sufficiently smooth functions and change insignificantly on scales determined by the scattering time and mean free path of conduction electrons, we can use the gradient expansion, which takes the nonlocal nature of the response function into account approximately. In that case, the nonequilibrium spin polarization can be represented in the form

$$s_\alpha = g_{\alpha\beta}\partial_t m_\beta + \mathcal{K}_{\alpha\beta}E_\beta + \mathcal{R}_{\alpha\beta\gamma\delta}E_\beta\nabla_\gamma m_\delta + \ldots\,. \tag{3}$$

The first term here determines the contribution of conduction electrons to the Gilbert damping, and the second and third terms refer to spin-orbit and spin-transfer torques, in full agreement with the established classification discussed above.

Calculation of the response function. As we have noted, the collective dynamics of a magnetic material is described by Eqn (2), which corresponds to the microscopic Landau–Lifshitz–Gilbert equation

$$\frac{\partial \mathbf{m}}{\partial t} = \gamma\mathbf{h}_{\mathrm{eff}} \times \mathbf{m} + \mathbf{T}\,, \tag{4}$$

where γ is the gyromagnetic ratio and $\mathbf{h}_{\mathrm{eff}} = -\delta\mathcal{F}/\delta\mathbf{m}$ is the effective magnetic field created by localized electrons, which is to be found from the expression for the micromagnetic energy $\mathcal{F}[\mathbf{m}]$, usually written using the Heisenberg model. With expansion (3), the term $\mathbf{T} = \kappa\mathbf{s} \times \mathbf{m}$ with $\kappa = \Delta_{\mathrm{sd}}\mathcal{A}/\hbar$ on the right-hand side collects the so-called spin torques.

To write the $g_{\alpha\beta}$, $\mathcal{K}_{\alpha\beta}$, and $\mathcal{R}_{\alpha\beta\gamma\delta}$ tensors in Eqn (3) explicitly, we assume that H_0 is the Hamiltonian of conduction electrons and consider the response of the spin density $\mathbf{s}(\mathbf{r}, t)$ to (1) slow deviation of the magnetization vector from the equilibrium position $\delta\mathbf{m}(\mathbf{r}, t) \approx (t - t_0)\partial_t\mathbf{m}$ and to the external electric field $\mathbf{E}(t)$ for (2) a uniform $\mathbf{m}$ and (3) a nonuniform magnetization profile $\delta\mathbf{m}(\mathbf{r}, t) \approx (\mathbf{r} - \mathbf{r}_0)\nabla_{\mathbf{r}}\mathbf{m}$. Cases 1 and 3 correspond to the presence of a perturbation $\delta U(\mathbf{r}, t) = -\Delta_{\mathrm{sd}}\boldsymbol{\sigma}\,\delta\mathbf{m}(\mathbf{r}, t)$ in the Hamiltonian, as follows from the expression for the s–d exchange interaction, and in case 2 this contribution is $\delta U(\mathbf{r}, t) = -\mathbf{j}\mathbf{A}/c$, where $\mathbf{j}$ is the current density vector, $\mathbf{A}(t)$ is the vector potential of the external electromagnetic field, and c is the speed of light in a vacuum.

As a relaxation mechanism, we consider scattering on scalar Gaussian disorder, which is defined by the correlator $\langle V(\mathbf{r}_1)V(\mathbf{r}_2)\rangle = V_0\delta(\mathbf{r}_1 - \mathbf{r}_2)$. In the case of a ferromagnetic material, we choose $V_0 = \hbar^2/(m_{\mathrm{e}}\tau)$, and in the case of an antiferromagnetic material, $V_0 = 2\pi\alpha_{\mathrm{d}}(\hbar v)^2$, where m_{e} and τ are the electron mass and scattering time, and v and α_{d} are the characteristic velocity and the relative strength of disorder.

The spin polarization of conduction electrons at a point $\mathbf{r}$ and time t can be calculated using its explicit definition in terms of Green's functions,

$$\delta s_\alpha(\mathbf{r}, t) = -\frac{\mathrm{i}}{2}\,\mathrm{Tr}\left[\sigma^\alpha\delta\mathcal{G}^<(\mathbf{r}t, \mathbf{r}t)\right], \tag{5}$$

where $\mathcal{G}^< = (\mathcal{G}^{\mathrm{K}} - \mathcal{G}^{\mathrm{R}} + \mathcal{G}^{\mathrm{A}})/2$ can be expressed in terms of the Keldysh $\mathcal{G}^{\mathrm{K}}$, the retarded $\mathcal{G}^{\mathrm{R}}$, and the advanced $\mathcal{G}^{\mathrm{A}}$ Green's functions of conduction electrons. If the system is located in the field of some potential $\delta U(\mathbf{r}, t)$, then, using the explicit form of the Dyson equation, in the first order of the perturbation theory, we can obtain

$$\delta\mathcal{G}(\mathbf{r}_1t_1, \mathbf{r}_2t_2) = \int \mathrm{d}^2r \oint_{\mathcal{C}_{\mathrm{K}}} \mathrm{d}t\; G(\mathbf{r}_1t_1, \mathbf{r}t)\delta U(\mathbf{r}t)G(\mathbf{r}t, \mathbf{r}_2t_2)\,, \tag{6}$$

where integration along the Keldysh contour $\mathcal{C}_{\mathrm{K}}$ is assumed, $G(\mathbf{r}_1t_1, \mathbf{r}_2t_2) = G(\mathbf{r}_1 - \mathbf{r}_2, t_1 - t_2)$ is the one-particle Green's function of conduction electrons, and

$$\hat{G} = \begin{pmatrix} \hat{G}^{\mathrm{R}} & \hat{G}^{\mathrm{K}} \\ 0 & \hat{G}^{\mathrm{A}} \end{pmatrix}, \qquad \hat{G}^{\mathrm{R}}(\varepsilon) = (\varepsilon - \hat{H}_0 + \mathrm{i}0)^{-1}\,, \tag{7}$$

where ε is the energy. Using (6), we can obtain the correction

$$\delta\mathcal{G}^<(\mathbf{r}t, \mathbf{r}t) = \int \mathrm{d}^2\tilde{r}\int_{-\infty}^{\infty} \mathrm{d}\tilde{t}\left[G^{\mathrm{R}}(\mathbf{r}t, \tilde{\mathbf{r}}\tilde{t})\delta U(\tilde{\mathbf{r}}\tilde{t})G^<(\tilde{\mathbf{r}}\tilde{t}, \mathbf{r}t) + G^<(\mathbf{r}t, \tilde{\mathbf{r}}\tilde{t})\delta U(\tilde{\mathbf{r}}\tilde{t})G^{\mathrm{A}}(\tilde{\mathbf{r}}\tilde{t}, \mathbf{r}t)\right]. \tag{8}$$

It is worth noting that, for equilibrium systems, using the fluctuation–dissipation theorem and Wigner transformation, we have

$$G_{\mathbf{p}}^<(\varepsilon) = \left[G_{\mathbf{p}}^{\mathrm{A}}(\varepsilon) - G_{\mathbf{p}}^{\mathrm{R}}(\varepsilon)\right]f(\varepsilon) = \int_{-\infty}^{\infty} \mathrm{d}t\; G_{\mathbf{p}}^<(t)\exp\left(\frac{\mathrm{i}\varepsilon t}{\hbar}\right). \tag{9}$$

Here, we introduce the Fermi–Dirac distribution $f(\varepsilon) = 1/\{1 + \exp[(\varepsilon - \mu)/T]\}$, where μ is the chemical potential and T is the temperature expressed in energy units (i.e., we set the Boltzmann constant $k_{\mathrm{B}} = 1$).

We consider the case where the system is placed in a monochromatic electromagnetic field $\mathbf{E}(t) = \mathbf{E}\exp(-\mathrm{i}\omega t)$. The potential then becomes $\delta U(t) = \mathrm{i}U_0\exp(-\mathrm{i}\omega t)/\omega$, where $U_0 = \mathbf{jE}$, $\mathbf{j} = -e\nabla_{\mathbf{p}}H_0$, and e is the electron charge. Calculating the correction by formula (8) leads to

$$\delta\mathcal{G}^{<}(\mathbf{r}t,\mathbf{r}t) = -\frac{\mathrm{i}\exp(-\mathrm{i}\omega t)}{\omega}\int\frac{\mathrm{d}^2p}{(2\pi)^2}\int_{-\infty}^{\infty}\frac{\mathrm{d}\varepsilon}{2\pi}\left[G^{\mathrm{R}}_{\mathbf{p}}(\varepsilon_+)\right.$$
$$\left.\times\, U_0G^{<}_{\mathbf{p}}(\varepsilon_-) + G^{<}_{\mathbf{p}}(\varepsilon_+)U_0G^{\mathrm{A}}_{\mathbf{p}}(\varepsilon_-)\right], \qquad (10)$$

where $\varepsilon_\pm = \varepsilon \pm \hbar\omega/2$. Taking the constant-field limit $\omega \to 0$, we can represent formula (9) as

$$\delta\mathcal{G}^{<}(\mathbf{r}t,\mathbf{r}t) = \int\frac{\mathrm{d}^2p}{(2\pi)^2}\int_{-\infty}^{\infty}\frac{\mathrm{d}\varepsilon}{2\pi}\left[\delta\mathcal{G}^{(1)} + \delta\mathcal{G}^{(2)}\right]. \qquad (11)$$

The obtained expression corresponds to the so-called Kubo–Streda formula, where the term

$$\delta\mathcal{G}^{(1)} = \frac{f(\varepsilon)}{2\mathrm{i}}\left[G^{\mathrm{R}}U_0\frac{\partial G^{\mathrm{R}}_{\mathbf{p}}}{\partial\varepsilon} - \frac{\partial G^{\mathrm{R}}_{\mathbf{p}}}{\partial\varepsilon}U_0G^{\mathrm{R}} - (\mathrm{R}\leftrightarrow\mathrm{A})\right], \quad (12)$$

called the Streda contribution [56], is due to the integration over all values of ε, and the term

$$\delta\mathcal{G}^{(2)} = \mathrm{i}\,\frac{\partial f(\varepsilon)}{\partial\varepsilon}\left[G^{\mathrm{R}}U_0G^{\mathrm{A}} - \frac{1}{2}\,G^{\mathrm{R}}U_0G^{\mathrm{R}} - \frac{1}{2}\,G^{\mathrm{A}}U_0G^{\mathrm{A}}\right] \qquad (13)$$

defines integration over the Fermi surface, which at $T = 0$ reduces to replacing ε with the Fermi energy ε_{F}. In Eqns (12) and (13), we introduce the notation $G^{\mathrm{R|A}} = G^{\mathrm{R|A}}_{\mathbf{p}}(\varepsilon)$ for brevity.

It is noteworthy that each term in (12) is a product of retarded or advanced Green's functions. The poles of the integrand lie on the same side of the imaginary plane, making the Streda contribution small in the limit of weak disorder [37, 57]. However, having no classical analogue, this contribution is quite important when the system spectrum has a gap and the Fermi energy is located exactly in the gap, as we discuss below. In analytic calculations, we assume that the Fermi energy is located sufficiently far from the gap; in other words, we work in the metallic regime and neglect Streda correction (12). Similar reasoning can be applied to the last two terms in (13), and therefore the spin-orbit torques in the system are mainly determined by the tensor [37]

$$\mathcal{K}_{\alpha\beta} = \frac{e}{4\pi}\int\frac{\mathrm{d}^2p}{(2\pi)^2}\,\mathrm{Tr}\left[\sigma_\alpha g^{\mathrm{R}}v^{\mathrm{vc}}_\beta g^{\mathrm{A}}\right]. \qquad (14)$$

It was assumed in deriving expression (14) that the magnetization can be considered almost uniform on scales determined by the mean free path of an electron. Similar calculations at $T = 0$ in a constant electric field $\mathbf{E}$, in accordance with the Kubo formula, yield the spin-transfer torques [54]

$$\mathcal{R}_{\alpha\beta\gamma\delta} = \mathrm{i}\,\frac{e\mathcal{A}\Delta^2_{\mathrm{sd}}}{2\pi\hbar S}\int\frac{\mathrm{d}^2p}{(2\pi)^2}\,\mathrm{Tr}\left[g^{\mathrm{A}}\hat{T}^{\mathrm{vc}}_\alpha g^{\mathrm{R}}v^{\mathrm{vc}}_\beta g^{\mathrm{A}}\sigma_\delta g^{\mathrm{A}}v_\gamma - \mathrm{h.c.}\right], \qquad (15)$$

where the velocity operator $\mathbf{v}$, as in (14), acquires the superscript vc corresponding to the value of the operator with the vertex correction due to summation over the impurity ladder. In turn, $g^{\mathrm{R/A}} = \langle G^{\mathrm{R/A}}\rangle$ is the disorder-averaged Green's functions of the conduction electrons, and $\mathbf{T} = \boldsymbol{\sigma}\times\mathbf{m}$. Finally, the Gilbert damping is expressed as [54]

$$g_{\alpha\beta} = \frac{\mathcal{A}\Delta^2_{\mathrm{sd}}}{2\pi\hbar^2 S}\int\frac{\mathrm{d}^2p}{(2\pi)^2}\,\mathrm{Tr}\left[g^{\mathrm{A}}\hat{T}^{\mathrm{vc}}_\alpha g^{\mathrm{R}}\sigma_\beta\right]. \qquad (16)$$

3. Two-dimensional Rashba ferromagnet

In this section, we review the results for a two-dimensional ferromagnet with a strong Rashba spin-orbit coupling obtained with the approach presented in Section 2.

3.1 Dzyaloshinskii–Moriya interaction

From the microscopic standpoint, the appearance of the Dzyaloshinskii–Moriya interaction in crystals without inversion, a possibility first noted in [58], is due to the presence of spin-orbit coupling [59]. To determine its strength in systems with magnetic order, it suffices to consider the s–d model described in Section 2 with the Hamiltonian of conduction electrons given by

$$H = \xi_p + \alpha_{\mathrm{R}}\zeta_p[\mathbf{p}\times\boldsymbol{\sigma}]_z + \Delta_{\mathrm{sd}}\mathbf{m}(\mathbf{r},t)\boldsymbol{\sigma}, \qquad (17)$$

where ξ_p and ζ_p, which are analytic functions of the absolute value of the momentum $\mathbf{p} = (p_x, p_y)$, determine the kinetic energy and the Rashba spin-orbit coupling, characterized by the parameter α_{R}. As in the foregoing, the last term on the right-hand side of (17) corresponds to the effective s–d exchange interaction strength Δ_{sd}, and the vector of Pauli matrices $\boldsymbol{\sigma}$ acts on spin indices. Assuming that the ferromagnetic material is at a temperature much lower than its Curie temperature, we can describe the localized magnetic moments in terms of a continuous vector field of unit length, $|\mathbf{m}(\mathbf{r},t)| = 1$.

In the continuum limit, the contribution of the Dzyaloshinskii–Moriya antisymmetric exchange interaction to the micromagnetic free energy density is given by $w_{\mathrm{DM}} = D(\Lambda^{(y)}_{yz} - \Lambda^{(x)}_{zx})$, where the parameter D is the coupling strength and $\Lambda^{(k)}_{ij} = m_i\nabla_k m_j - m_j\nabla_k m_i$ are the Lifshitz invariants. It is easy to see that the coupling w_{DM} is linear in the first spatial derivatives of the magnetization vector $\mathbf{m}$. In turn, the symmetric exchange interaction $w_{\mathrm{ex}} = A(|\nabla_x\mathbf{m}|^2 + |\nabla_y\mathbf{m}|^2)$, whose strength is determined by the parameter A, is due to terms that are quadratic in the first spatial derivatives of $\mathbf{m}$. We note that the relation between D and A plays a key role in the formation of chiral magnetic structures, such as a magnetic skyrmion or a magnetic soliton, determining their stability and size [43, 44].

To find the contribution from the Dzyaloshinskii–Moriya interaction, we use the expansion of the grand thermodynamic potential Ω and keep the terms that are linear in the first spatial derivatives of the magnetization vector; this allows us not to assume a priori the symmetry of the final result. The density of the thermodynamic potential Ω at a point $\mathbf{r}$ is given by

$$\Omega = -T\int\frac{\mathrm{d}\varepsilon}{2\pi\mathrm{i}}\,\mathrm{Tr}\left[\mathcal{G}^{\mathrm{A}}(\mathbf{r},\mathbf{r}) - \mathcal{G}^{\mathrm{R}}(\mathbf{r},\mathbf{r})\right]g(\varepsilon), \qquad (18)$$

where

$$g(\varepsilon) = \ln\{1 + \exp[(\mu-\varepsilon)/T]\} \;\text{ and }\; \mathcal{G}^{\mathrm{R|A}} = (\varepsilon - H \pm \mathrm{i}0)^{-1}$$

are the retarded and advanced Green's functions for the system with Hamiltonian (17), respectively. Using the

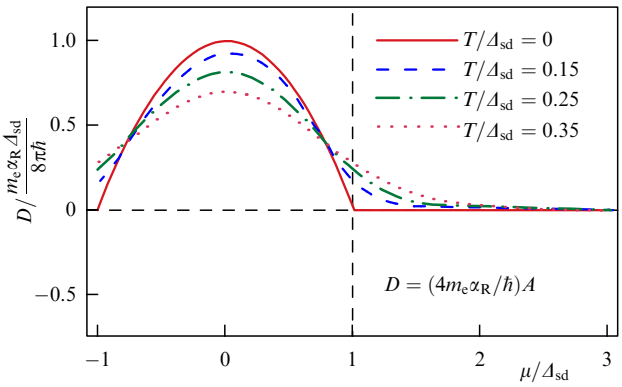

Figure 1. Dzyaloshinskii–Moriya interaction in a two-dimensional Rashba ferromagnet obtained by solving Eqn (21) numerically at various temperatures. Antisymmetric exchange interaction constant D is nonzero only in the semimetallic regime at $T = 0$, while, as the temperature increases, the Dzyaloshinskii–Moriya interaction also manifests itself in the metallic phase [46].

Dyson equation, in the first order of the perturbation theory, we find the function

$$\Omega[\mathbf{m}] = \sum_{\alpha\beta} \Omega_{\alpha\beta}^{\mathrm{DM}} \nabla_\alpha m_\beta \,. \tag{19}$$

Expression (19) is obtained upon inclusion of small deviations of the magnetization vector $\mathbf{m}(\mathbf{r}) \approx \mathbf{m}(\mathbf{r}_0) + (\mathbf{r} - \mathbf{r}_0)\nabla_{\mathbf{r}}\mathbf{m}(\mathbf{r}_0)$ from equilibrium in the last term in (17). For simplicity in what follows, we assume that $\mathbf{m} = \mathbf{m}(\mathbf{r}_0)$ hereafter.

The tensor $\Omega_{\alpha\beta}^{\mathrm{DM}}$ in (19) can be found explicitly from

$$\Omega_{\alpha\beta}^{\mathrm{DM}} = \frac{T\Delta_{\mathrm{sd}}}{2\pi\hbar}\,\mathrm{Re}\int g(\varepsilon)\,\mathrm{d}\varepsilon \int \frac{\mathrm{d}^2 p}{(2\pi)^2} \times \mathrm{Tr}\left[G^{\mathrm{R}}\sigma_\beta G^{\mathrm{R}} v_\alpha G^{\mathrm{R}} - G^{\mathrm{R}} v_\alpha G^{\mathrm{R}}\sigma_\beta G^{\mathrm{R}}\right], \tag{20}$$

where G^{R} is the retarded Green's function for Hamiltonian (17) with a uniform background magnetization $\mathbf{m}$, and we introduce the velocity $\mathbf{v} = \nabla_{\mathbf{p}} H$ [46]. With this relation, the Dzyaloshinskii–Moriya coupling strength can be expressed as

$$D = \frac{\alpha_{\mathrm{R}}\Delta_{\mathrm{sd}}}{8\pi\hbar}\,\frac{\partial}{\partial\Delta_{\mathrm{sd}}}\left(\int_0^\infty \frac{f_- - f_+}{\Delta_{\mathrm{sd}}}\,\zeta_p\xi_p' p^2\,\mathrm{d}p\right), \tag{21}$$

where $f_\pm = f(\xi_p \pm \Delta_{\mathrm{sd}})$, $f(\varepsilon)$ is the Fermi–Dirac distribution, and $\xi_p' = \partial\xi_p/\partial p$. In particular, for the Bychkov–Rashba model with a quadratic law $\xi_p = p^2/(2m_{\mathrm{e}})$ and $\zeta_p = 1$ at $T = 0$, we obtain

$$D = \frac{m_{\mathrm{e}}\alpha_{\mathrm{R}}\Delta_{\mathrm{sd}}}{8\pi\hbar}\left(1 - \frac{\mu^2}{\Delta_{\mathrm{sd}}^2}\right) \quad \text{at} \quad |\mu| < \Delta_{\mathrm{sd}}\,, \tag{22}$$

and $D = 0$ otherwise. We note that, in the Bychkov–Rashba model, the symmetric and antisymmetric exchange interaction constants are related as $A = \hbar D/(4m_{\mathrm{e}}\alpha_{\mathrm{R}})$ [46].

In Fig. 1, we show the results of numerical integration of (21) for the antisymmetric exchange interaction constant in the two-dimensional Rashba magnet as a function of temperature. In the limit of zero temperature $T = 0$, as we can see, the Dzyaloshinskii–Moriya coupling constant D is nonzero only in the semimetallic regime $|\mu/\Delta_{\mathrm{sd}}| < 1$, which coincides with the results of analytic calculations in the Bychkov–Rashba model.

3.2 Spin-orbit torques

We return to the model of conduction electrons with Hamiltonian (17), choose the $\hat{\mathbf{z}}$-axis perpendicular to the plane of the structure under consideration, and assume that the ferromagnetic material is located in the plane $z = 0$. For a current directed in the magnetic structure plane, we can use expression (14) to calculate the spin-orbit torques in the system.

Before proceeding with a discussion of the results, we note that the symmetry analysis of model (17) with the Rashba spin-orbit coupling allows concluding that the spin-orbit torques are characterized in the general case by four coefficients, which, within the phenomenological approach, are unknown functions of the magnetization vector components [41]. Indeed, the spin-orbit torques can be represented as $\mathbf{T}^{\mathrm{SOT}} = \mathbf{T}_{\parallel}^{\mathrm{SOT}} + \mathbf{T}_{\perp}^{\mathrm{SOT}}$, where

$$\mathbf{T}_{\parallel}^{\mathrm{SOT}} = a\mathbf{m}\times(\hat{\mathbf{z}}\times\mathbf{E}) + c\mathbf{m}\times(\mathbf{m}\times\hat{\mathbf{z}})(\mathbf{m}\mathbf{E}) \tag{23}$$

defines the dissipative (damping-like) contribution to the spin-orbit torques, in other words, changes sign under time reversal, and

$$\mathbf{T}_{\perp}^{\mathrm{SOT}} = b\mathbf{m}\times\big(\mathbf{m}\times(\hat{\mathbf{z}}\times\mathbf{E})\big) + d(\mathbf{m}\times\hat{\mathbf{z}})(\mathbf{m}\mathbf{E}) \tag{24}$$

corresponds to a field-like contribution that is even under time reversal. Here, $\mathbf{E} = (E_x, E_y)$ is the electric field strength vector oriented parallel to the plane of the sample. Interestingly, the functional dependence of the coefficients $a(\theta)$, $b(\theta)$, $c(\theta)$, and $d(\theta)$ is determined only by the polar angle formed by the magnetization vector and the $\hat{\mathbf{z}}$-axis. We note that in the metallic regime $\varepsilon_{\mathrm{F}} \gg \hbar/\tau$, where τ is the characteristic electron scattering time, these coefficients take almost constant values, regardless of the disorder model used in the calculations.

We assume the most general orientation of the magnetization vector and choose a coordinate system such that the x-axis coincides with the projection of the magnetization vector onto the plane of the ferromagnetic material: $\mathbf{m} = (m_x, 0, m_z)$. We then treat the addition due to $\Delta_{\mathrm{sd}} m_x\sigma_x$ perturbatively. The expansion in a perturbative series in this case is equivalent to the expansion in powers of $m_x\Delta_{\mathrm{sd}}/\Delta_{\mathrm{S}}$, where $\Delta_{\mathrm{S}} = (m_z^2\Delta_{\mathrm{sd}}^2 + 2\varepsilon_{\mathrm{F}} m_{\mathrm{e}}\alpha_{\mathrm{R}}^2)^{1/2}$ [37]. For sufficiently well-separated subbands, $\Delta_{\mathrm{S}} \gg \hbar/\tau$, the coefficients b and d are less than a and c in Eqns (23) and (24). Explicitly, we have

$$a = \kappa m_{\mathrm{e}}\frac{e\tau\alpha_{\mathrm{R}}}{4\pi\hbar}\left[1 + \mu_z^2 - \mu_x^2\mu_z^2(1 + 3\mu_z^2)\right], \tag{25}$$

$$b = \kappa m_{\mathrm{e}}\frac{e\alpha_{\mathrm{R}}}{4\pi}\,\frac{\hbar\Delta_{\mathrm{sd}}}{\Delta_{\mathrm{S}}^2}\left[1 + \mu_x^2(1 - 2\mu_z^2)\right], \tag{26}$$

$$c = -\kappa m_{\mathrm{e}}\mu_z^2\,\frac{e\tau\alpha_{\mathrm{R}}}{4\pi\hbar}\,\frac{\Delta_{\mathrm{sd}}^2}{\Delta_{\mathrm{S}}^2}\left[3 + \mu_z^2 + 2\mu_x^2(2 - 3\mu_z^2)\right], \tag{27}$$

$$d = \kappa m_{\mathrm{e}}\frac{e\alpha_{\mathrm{R}}}{4\pi}\,\frac{\hbar\Delta_{\mathrm{sd}}}{\Delta_{\mathrm{S}}^2}\left[1 + \mu_z^2 - 3\mu_z^4 - \mu_x^2(1 - 3\mu_z^2) + \frac{2\Delta_{\mathrm{sd}}^2}{\Delta_{\mathrm{S}}^2}(1 - 2\mu_z^2)\right], \tag{28}$$

with the vector $\boldsymbol{\mu} = \Delta_{\mathrm{sd}}\mathbf{m}/\Delta_{\mathrm{S}}$. It is easy to see from the expressions for the coefficients that, for $\Delta_{\mathrm{sd}} \ll \Delta_{\mathrm{S}}$, the dependence on the polar angle becomes weak and the parameters a, b, c, and d take approximately constant values. In turn, a and c explicitly depend on the scattering time τ, which, as noted above, determines the dissipative character of $\mathbf{T}_{\parallel}^{\mathrm{SOT}}$.

Although the above results are universal, i.e., are independent of the nature of disorder, a limitation of this approach is the fact that the correlator $\mathcal{K}_{\alpha\beta}$ was calculated in the approximation of disjoint diagrams. But, as demonstrated in [60, 61], the microscopic analysis of such correlators should also include oblique scattering on rare impurity configurations with the distance between some two impurities being comparable to the de Broglie wavelength of an electron. However, we emphasize that the calculation in the framework of the self-consistent Born approximation, as implemented above, is fully consistent in the leading order in $\varepsilon_F \gg \hbar/\tau$.

We note that the results obtained for spin-orbit torques are exact in the metallic limit $\varepsilon_F > \Delta_{sd}$, when we can neglect Streda's topological contribution (12) in view of the vanishingly small Berry curvature.

We also emphasize the following. In the absence of spin-orbit coupling ($\alpha_R = 0$), the nonequilibrium spin polarization of conduction electrons $\delta\mathbf{s}$ in Eqn (5) becomes proportional to the number of electrons in the direction of the magnetization vector $\mathbf{m}$ of the sample, which can be interpreted as the occurrence of a diffusion pole in calculations of the corresponding diagrams, and which requires vertex corrections to be carefully taken into account. It turns out that all orders in m_x can be formally taken into account by writing the velocity operator with the summation over the impurity ladder in (14) and with the corresponding Green's functions replaced with those accounting for disorder, which results in the following expression for the spin-orbit torque tensor:

$$\mathcal{K} = \frac{e m_e \alpha_R}{2\pi} \begin{pmatrix} 0 & \tau \\ -\tau & 0 \\ 0 & 0 \end{pmatrix}. \tag{29}$$

It is easy to see that the tensor $\mathcal{K}$ is independent of the exchange interaction strength and of the orientation of the magnetization vector, and has nonzero components even in the absence of the s–d exchange interaction in the system [62–64].

3.3 Spin-transfer torques

We next discuss the mechanism of generation of spin-transfer torques, where the magnetization $\mathbf{m}$ of the structure causes the spins of electrons drifting under the influence of an external electric field $\mathbf{E}$ in the substrate or in the magnetic material itself to polarize and then affect the dynamics of the magnetization vector. As a model system, we choose a two-dimensional ferromagnet with the Rashba spin-orbit coupling described by Hamiltonian (17) in the presence of scalar Gaussian disorder. Below, we review the most significant theoretical results obtained, as in the case of spin-orbit torques, under the assumption of a metallic regime.

For an arbitrary orientation of the magnetization vector in a two-dimensional Rashba ferromagnet, the spin-transfer torques

$$\mathbf{T}^{STT} = \xi_0 \partial_{\mathbf{v}} \mathbf{m} - \xi_\parallel (\mathbf{m} \times \partial_{\mathbf{v}} \mathbf{m}_\parallel) - \xi_\perp (\mathbf{m} \times \partial_{\mathbf{v}} \mathbf{m}_\perp) \tag{30}$$

and the Gilbert damping

$$\mathbf{T}^{GD} = \xi_0 \partial_t \mathbf{m} - \xi_\parallel (\mathbf{m} \times \partial_t \mathbf{m}_\parallel) - \xi_\perp (\mathbf{m} \times \partial_t \mathbf{m}_\perp) \tag{31}$$

are defined by the coefficients $\xi_i = \xi_i(\mathbf{m})$, where $\partial_{\mathbf{v}} = (\mathbf{v}_d \nabla)$, $\mathbf{v}_d = e\hbar\tau\mathbf{E}/m$ is the classical electron drift velocity in an electric field, and $\mathbf{m} = \mathbf{m}_\parallel + \mathbf{m}_\perp$ with $\mathbf{m}_\perp = \hat{\mathbf{z}} \cos\theta$. We note that, for the convenience, the term $\xi_0 \partial_t \mathbf{m}$ was included in the definition of Gilbert damping (31), but, because of the parity of this term under time reversal, its effect reduces to spin renormalization in the Landau–Lifshitz–Gilbert equation, i.e., it does not lead to actual damping. We mention specifically that we have chosen Gaussian disorder as a physical mechanism responsible for momentum relaxation. This is because, just like the spin-transfer torques, both the conductivity tensor and the Gilbert damping contain essentially dissipative components.

The rotational and orientational anisotropies appearing in the expression for the spin torques are a consequence of the fact that the Rashba-type spin-orbit coupling highlights a direction perpendicular to the two-dimensional plane of the structure. The orientational anisotropy of $\xi_i(\mathbf{m})$ is determined by all elements of the space symmetry group of the system. For $C_{\infty v}$, i.e., in model (17), the coefficients $\xi_i(m_z)$ are determined only by the polar angle of the magnetization vector. It is easy to see that the expression for spin torques contains both the adiabatic contribution $\propto (\mathbf{E}\nabla)\mathbf{m}$ and the nonadiabatic contribution $\propto \mathbf{m} \times (\mathbf{E}\nabla)\mathbf{m}$. In the absence of spin-orbit coupling in the system, the physical interpretation of the adiabatic contribution becomes transparent and intuitively clear: because the spins of the conduction electrons adiabatically follow the direction of the local magnetization, the corresponding change in their angular momentum is transferred to the magnetic texture.

Another remarkable property of the introduced expressions in form (30) and (31) is that they yield a simple and exact relation between the nonadiabatic spin-transfer torque and the Gilbert damping, which is important for the current-induced motion of magnetic textures, including domain walls and skyrmions. Indeed, in a moving reference frame, both components of the nonadiabatic torque, determined by the coefficients $\xi_\parallel$ and $\xi_\perp$, are canceled by the corresponding terms in the expression for Gilbert damping. Therefore, if the influence of other torques on the motion of the magnetic texture is insignificant, then its final velocity in the moving reference frame must disappear in the absence of a magnetic field. This means that in the laboratory reference frame the texture moves with the universal electron drift velocity v_d. Therefore, it seems more convenient to study the dynamics of a magnetic texture in a moving reference frame, where nonadiabatic torque contribution associated with the spin transfer is absent.

The coefficients ξ_0, $\xi_\parallel$, and $\xi_\perp$, which determine the spin-transfer torques and Gilbert damping in accordance with (30) and (31), can be found by numerically integrating Eqn (15) for $\mathcal{R}_{\alpha\beta\gamma\delta}$. In particular, in Fig. 2 we show the values of the coefficients for three directions of $\mathbf{m}$, including the magnetization perpendicular to the structure plane ($\theta = 0$) and lying in the plane ($\theta = \pi/2$), as well as the general case (we choose $\theta = 2\pi/5$ for illustration); these coefficients are in full agreement with the asymptotic values [54] calculated for weak spin-orbit and weak s–d exchange interactions.

If the Rashba spin-orbit coupling is absent in the system ($\alpha_R = 0$), then both the contribution to the Gilbert damping due to conduction electrons and the nonadiabatic spin-transfer torque are absent, and

$$\xi_0 = \frac{\Delta_{sd} \mathcal{A} m}{2\pi\hbar^2 S}, \qquad \xi_\parallel = \xi_\perp = 0. \tag{32}$$

The parameter $\xi_0 = -\delta S_{eff}/S$ determines the effective spin renormalization in the Landau–Lifshitz–Gilbert equation,

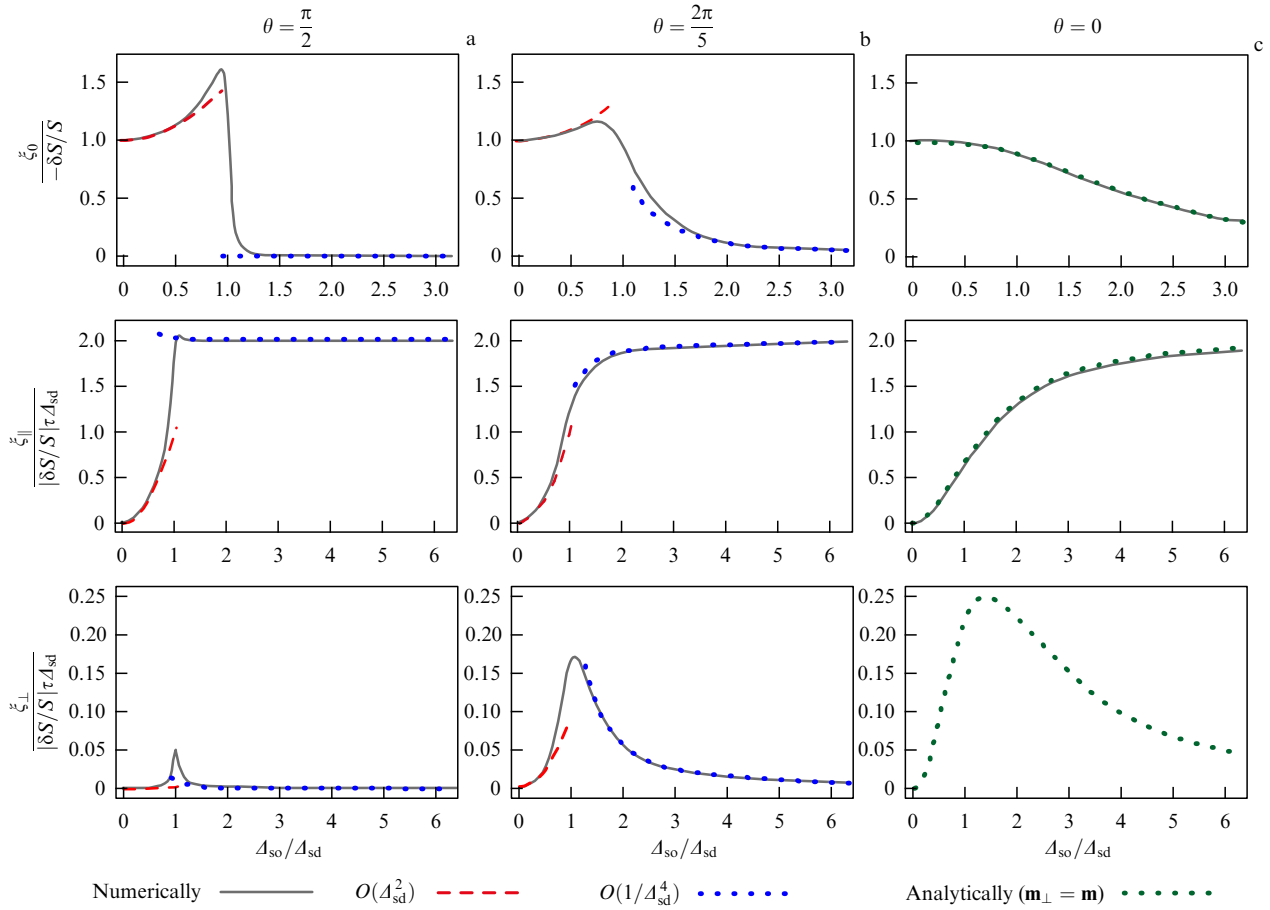

Figure 2. (Color online.) Coefficients ξ_0, $\xi_\parallel$, and $\xi_\perp$ determining spin-transfer torques and Gilbert damping in a two-dimensional Rashba ferromagnet for the magnetization vector (a) lying in the plane of the structure, $\theta = \pi/2$, (c) perpendicular to it, $\theta = 0$, and (b) having an arbitrarily chosen orientation $\theta = 2\pi/5$. Results of numerical integration of expression (15) are shown with a solid black curve. Two asymptotic cases [54] are distinguished corresponding to the limit of weak spin-orbit coupling (red dashed curve) and weak s–d exchange interaction (blue dots). For the magnetization vector perpendicular to the plane of the ferromagnet, exact analytic solution (34)–(36) can be found (green dots).

which physically means that a fraction of conduction electrons is associated with a localized moment. Indeed, in the absence of spin-orbit coupling, conduction electrons are polarized in the direction of the magnetization vector or in the opposite direction, and hence the total electron spin per unit cell can be exactly expressed as

$$\delta S = \delta S_\uparrow - \delta S_\downarrow = -\frac{\Delta_{sd}\mathcal{A}m}{2\pi\hbar^2} = -\xi_0 S. \tag{33}$$

If the magnetization vector of a ferromagnetic material is perpendicular to the structure plane, $\mathbf{m} = \mathbf{m}_\perp$, then

$$\xi_0 = -\frac{\delta S}{S}\left[1 - \frac{(\tau\Delta_{so}^2/\hbar)^2}{\Delta_{sd}^2 + \tau^2(2\Delta_{sd}^2 + \Delta_{so}^2)^2/\hbar^2}\right], \tag{34}$$

$$\xi_\parallel = \left|\frac{\delta S}{S}\right| \frac{\tau\Delta_{sd}}{\hbar} \frac{\Delta_{so}^2\left[1 + 2\tau^2(2\Delta_{sd}^2 + \Delta_{so}^2)/\hbar^2\right]}{\Delta_{sd}^2 + \tau^2(2\Delta_{sd}^2 + \Delta_{so}^2)^2/\hbar^2}, \tag{35}$$

$$\xi_\perp = \left|\frac{\delta S}{S}\right| \frac{\tau\Delta_{sd}}{2\hbar} \frac{\Delta_{so}^2\left[1 + (2\tau\Delta_{sd}/\hbar)^2\right]}{\Delta_{sd}^2 + \tau^2(2\Delta_{sd}^2 + \Delta_{so}^2)^2/\hbar^2}, \tag{36}$$

where $\Delta_{so} = \sqrt{2\varepsilon_F m_e \alpha_R^2}$. We note that, for a fixed direction $\mathbf{m} = \mathbf{m}_\perp$, we can make no conclusion about $\xi_\perp$, because this quantity determines the factor in front of $\mathbf{m} \times \partial\mathbf{m}_\perp$ and can in principle take an arbitrary value; nevertheless, an analytic expression for $\xi_\perp$ can be found in the limit $\theta \to 0$.

Concluding this section, we note that the formulas obtained here and below for the spin-orbit and spin-transfer torques can be equivalently represented in terms of the external electric current using the explicit expression $\mathbf{E} = \hat{\sigma}^{-1}\mathbf{j}$, where $\hat{\sigma}$ is the conductivity tensor of the material.

4. Two-dimensional Rashba antiferromagnet

A fully electrical switching of the Néel vector orientation in an antiferromagnetic material due to spin-orbit torques was predicted in [65] and detected in noncentrosymmetric CuMnAs [66–69] and Mn_2Au [70–72] crystals. Although many antiferromagnets are electrical insulators [73], which limits the range of their possible use, for example, for spin injection [74], materials such as CuMnAs and Mn_2Au have semimetallic and metallic properties, which determines the high conductivity of these structures and the presence of a strong spin-orbit coupling. Another important characteristic of these materials is that they allow the excitation of collective modes in the terahertz range [72].

The spin-orbit torque in antiferromagnets that is most interesting from the standpoint of practical applications has been studied theoretically using the Kubo–Streda formula in the case of a two-dimensional Rashba electron gas and in tight-binding models using Mn_2Au as an example [65, 75]. This laid the foundation for further studies of spin-orbit

torques in heterostructures made of antiferromagnets [76, 77]. We note that a symmetry analysis based on point magnetic groups of antiferromagnets has also been developed to predict the shape of spin-transfer torques [75, 78].

In Sections 4.1–4.4, we review results that allow determining the spin-transfer torques [51] and Gilbert damping [52] within the microscopic theory presented in Section 2. We especially note that, in contrast to calculations for a two-dimensional Rashba ferromagnet studied in detail in Section 3, the calculations of spin-transfer torques for a model antiferromagnet presented here are done via numerical simulations and are not limited to the metallic regime. Below, we consider the nonequilibrium spin polarization of conduction electrons for the effective s–d model of a two-dimensional Rashba antiferromagnet on a hexagonal lattice with a strong Rashba spin-orbit coupling and local scalar disorder. We show that, just as in two-dimensional ferromagnetic materials, the presence of spin-orbit coupling leads to a significant anisotropy of the spin torques [51] and Gilbert damping [52]. We also discuss exact analytic results obtained for spin torques in the case of antiferromagnetic metals, where calculations can be performed analytically [52].

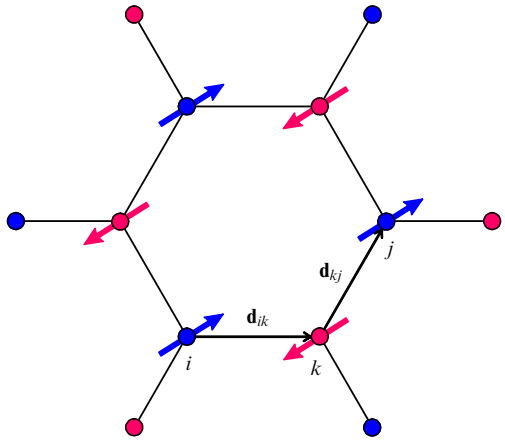

Figure 3. (Color online.) Two-dimensional Rashba antiferromagnet model on a hexagonal lattice with oppositely directed magnetization vectors on two sublattices, A and B, shown in blue and red, respectively. Vectors $\mathbf{d}_{ik}$ and $\mathbf{d}_{kj}$ connect neighboring lattice sites such that the beginning of vector $\mathbf{d}_{ij}$ is at the ith site and the end, at the jth.

4.1 Hamiltonian of the Rashba antiferromagnet

To illustrate the developed technique, we consider the s–d model of a two-dimensional antiferromagnet on a hexagonal lattice (Fig. 3), assuming that the conduction electrons are described by the Kane–Mele strong coupling model [79, 80]. The choice of the microscopic model is partly motivated by recent studies of CuMnAs [81]; we assume that the Fermi energy level of the conduction electrons remains near the Dirac points, and hence the Fermi surfaces are located near two valleys, K and K′. The Hamiltonian of the conduction electrons is therefore given by

$$H = H_0 + H_{\mathrm{R}} + H_{\mathrm{sd}}\,, \tag{37}$$

where H_0 is the Hamiltonian describing the hopping of conduction electrons between nearest neighbors,

$$H_0 = -w\sum_{\langle i,j\rangle}\sum_{\sigma} c^{\dagger}_{i\sigma}c_{j\sigma}\,, \tag{38}$$

with the hopping integral w, and $c_{i\sigma}$ and $c^{\dagger}_{i\sigma}$ are electron annihilation and creation operators with the spin projection σ on the ith site. The Rashba spin-orbit coupling

$$H_{\mathrm{R}} = \frac{\mathrm{i}\lambda}{a}\sum_{\langle i,j\rangle}\sum_{\sigma\sigma'}\hat{\mathbf{z}}(\boldsymbol{\sigma}\times\mathbf{d}_{ij})_{\sigma\sigma'}c^{\dagger}_{i\sigma}c_{j\sigma'} \tag{39}$$

is introduced by the parameter λ, a is the two-dimensional crystal lattice constant, the unit vector $\hat{\mathbf{z}}$ is perpendicular to the plane of the structure, and the components of the vector $\boldsymbol{\sigma} = (\sigma_x, \sigma_y, \sigma_z)$ are the corresponding Pauli matrices. For any sublattice sites A, the vectors $\mathbf{d}_{ij}$ connecting the nearest lattice sites can be defined as

$$\mathbf{d}_1 = a\begin{pmatrix}1\\0\end{pmatrix}, \qquad \mathbf{d}_2 = \frac{a}{2}\begin{pmatrix}-1\\\sqrt{3}\end{pmatrix}, \qquad \mathbf{d}_3 = -\frac{a}{2}\begin{pmatrix}1\\\sqrt{3}\end{pmatrix}.$$

The exchange interaction between localized magnetic moments $\mathbf{S}_i$ and conduction electron spins is described by

$$H_{\mathrm{sd}} = -J_{\mathrm{sd}}\sum_{i}\sum_{\sigma\sigma'}\mathbf{S}_i\,\boldsymbol{\sigma}_{\sigma\sigma'}c^{\dagger}_{i\sigma}c_{i\sigma'}\,, \tag{40}$$

where the exchange interaction strength J_{sd} is chosen to be the same for both sublattices. Importantly, expression (40) relates the model of conduction electrons formulated in the tight-binding approximation to the classical Heisenberg Hamiltonian of localized magnetic moments $\mathbf{S}_i$, whose ground state corresponds to antiferromagnetic ordering. In what follows, we assume that $|\mathbf{S}_i| = S \gg 1$, and the characteristic s–d exchange energy is given by $\Delta_{\mathrm{sd}} = J_{\mathrm{sd}}S$ (as for a ferromagnet).

In subsequent calculations, we consider a single-domain antiferromagnetic material with a unit Néel vector $\mathbf{n} = (\mathbf{S}_{\mathrm{A}} - \mathbf{S}_{\mathrm{B}})/(2S)$. It is easy to see that the model in (37)–(40) guarantees the symmetry with respect to the sublattices ($\mathrm{A} \leftrightarrow \mathrm{B}$), ensured by the equality of spin-orbit and s–d exchange interactions on both sublattices. The advantages of the high symmetry of the model include the total isotropy of the Fermi surface with respect to the azimuthal (in-plane) direction of the Néel vector $\mathbf{n}$. However, the band structure of the symmetric model strongly depends on the polar angle θ of the Néel vector, $n_z = \cos\theta$, as shown in Fig. 4.

The Hamiltonian H_{eff} of low-energy conduction electrons can be obtained by linearizing (37) in the vicinity of the valleys

$$\mathbf{K} = \frac{4\pi}{3\sqrt{3}a}\begin{pmatrix}0\\1\end{pmatrix}, \qquad \mathbf{K}' = -\mathbf{K}\,. \tag{41}$$

Recalling that $v = 3wa/(2\hbar)$ and $\mathbf{S}_{\mathrm{A}} = -\mathbf{S}_{\mathrm{B}}$, we have

$$H_{\mathrm{eff}} = v(\mathbf{p}\boldsymbol{\Sigma}) + \frac{\lambda}{2}[\boldsymbol{\sigma}\times\boldsymbol{\Sigma}]_z - \Delta(\mathbf{n}\boldsymbol{\sigma})\Sigma_z\Lambda_z + V(\mathbf{r})\,, \tag{42}$$

where $\boldsymbol{\Sigma}$, $\boldsymbol{\Lambda}$, and $\boldsymbol{\sigma}$ are vectors composed of the Pauli matrices acting, respectively, on the sublattice, valley, and spin indices.

It is worth noting that the term $V(\mathbf{r})$, which corresponds to the Gaussian disorder, implying that $\langle V(\mathbf{r})\rangle = 0$, and is fully characterized by the two-point correlator $\langle V(\mathbf{r})V(\mathbf{r}')\rangle = 2\pi(\hbar v)^2\alpha_{\mathrm{d}}\delta(\mathbf{r}-\mathbf{r}')$, where angular brackets denote averaging over disorder and the dimensionless parameter $\alpha_{\mathrm{d}} \ll 1$ defines the strength of disorder, leads to relaxation of the momentum of conduction electrons (see the discussion in Section 2). The exchange interaction and spin-orbit scattering (or scattering by noncollinear configurations with $\mathbf{m} = 0$) provide a link between localized magnetic moments and kinetic moments of

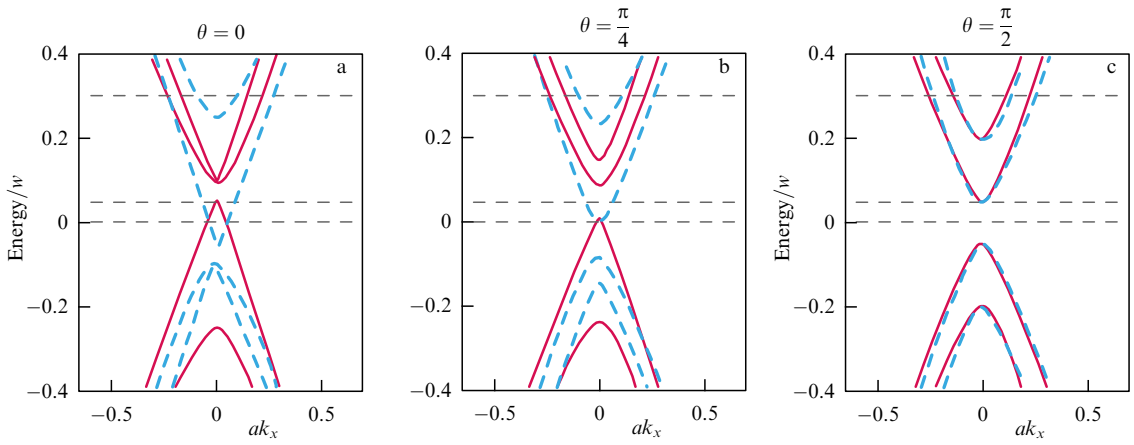

Figure 4. (Color online.) Band structure corresponding to Hamiltonian (37) for different orientations of the Néel vector: (a) perpendicular to the plane of the antiferromagnet, $\theta = 0$, (b) arbitrary, $\theta = \pi/4$, and (c) in the structure plane, $\theta = \pi/2$. Red curves correspond to the K valley, blue curves, to the K′ valley. Horizontal lines mark possible positions of the Fermi level ε_F that are characteristic of a dielectric ($\varepsilon_F = 0$), a semimetal ($\varepsilon_F = 0.05w$), or a metal ($\varepsilon_F = 0.3w$).

electrons. Both these mechanisms form a channel for scattering the angular momentum of localized spins into the lattice. Thus, the considered model provides us with a microscopic basis for studying dissipative quantities such as Gilbert damping, spin-orbit torques, and conductivity, which we discuss in what follows.

4.2 Spin-orbit torques

We note that effective model (42) is characterized by the point symmetry group $C_{\infty v}$. The second term in the model Hamiltonian H_{eff} can be interpreted as the Zeeman contribution $\hat{\mathbf{z}} \times \mathbf{j}$, where $\mathbf{j}$ is the electric current in the system, which we always assume to be oriented along the x-axis for simplicity. This field induces a nonequilibrium spin polarization of conduction electrons, in full analogy with how this occurs in ferromagnetic materials. With the point symmetry group

$$\begin{aligned}\delta\mathbf{s}^{+} = {} & A(n_z^2)\hat{\mathbf{z}} \times \mathbf{j} + A'(n_z^2)\mathbf{n}_{\parallel} \times \big(\mathbf{n}_{\parallel} \times (\hat{\mathbf{z}} \times \mathbf{j})\big) \\ & + B_{\perp}(n_z^2)\mathbf{n}_{\perp} \times (\hat{\mathbf{z}} \times \mathbf{j}) + B_{\parallel}(n_z^2)\mathbf{n}_{\parallel} \times (\hat{\mathbf{z}} \times \mathbf{j}) \\ & + C(n_z^2)\mathbf{n}_{\parallel} \times \big(\mathbf{n}_{\perp} \times (\hat{\mathbf{z}} \times \mathbf{j})\big)\,, \end{aligned} \tag{43}$$

where $\delta\mathbf{s}^{\pm} = (\delta\mathbf{s}^{\mathrm{A}} \pm \delta\mathbf{s}^{\mathrm{B}})/2$ are constructed from nonequilibrium spin polarizations of the two sublattices, we also split the Néel vector into the in-plane and perpendicular components: $\mathbf{n} = \mathbf{n}_{\parallel} + \mathbf{n}_{\perp}$. This representation of the spin polarization is dictated by two transformations: the Néel vector inversion $\mathbf{n} \to -\mathbf{n}$ and the reflection in the structure plane $\mathbf{n}_{\perp} \to -\mathbf{n}_{\perp}$. Because the model is isotropic with respect to in-plane rotations, only these symmetries determine the nonequilibrium spin polarization. The first two terms in (43) are even under both Néel vector inversion and reflection in the plane of the structure, and the last term is even under inversion but odd under reflection. These terms correspond to field-like torques, i.e., are invariant under time reversal. The third and fourth terms in formula (43) are odd and even, respectively, under inversion, but not odd under reflection, and hence represent antidamping-like spin-orbit torques that change sign under time reversal. In turn, the coefficients in front of the corresponding vector expressions are invariant with respect to $C_{\infty v}$ group, but can vary depending on n_z^2. In view of the symmetry of the model with respect to the sublattices, $\Lambda_x H_{\text{eff}}[-\mathbf{n}]\Lambda_x = H_{\text{eff}}[\mathbf{n}]$ and $\delta\mathbf{s}^{-} = 0$, which results in the vanishing of the antidamping contributions, $B_{\perp} = B_{\parallel} = 0$. It is also worth noting that expression (43) is equivalent to (23), (24), with the only difference that we have switched from the components of the electric field strength vector $\mathbf{E}$ to the electric current density vector $\mathbf{j}$ using Ohm's law in differential form, expressed in terms of the conductivity tensor.

We consider possible scenarios for estimating the magnitude of the nonequilibrium spin polarization of conduction electrons depending on the Fermi level position in the system shown schematically in Fig. 5. In the metallic regime, when there are two Fermi surfaces in each valley, the coefficients A, A', and C as functions of the Néel vector direction are shown in Fig. 6. As can be seen, the contribution of higher harmonics to the nonequilibrium spin polarization, being proportional to the expansion coefficients A' and C, is negligible, which leads to

$$\delta\mathbf{s}^{+} \propto A\hat{\mathbf{z}} \times \mathbf{j} \tag{44}$$

with a dimensionless coefficient A, whose value remains almost constant regardless of the impurity concentration (Fig. 7). Expression (44), as can be easily seen, corresponds to the inverse spin–galvanic Edelstein effect [62], which, as discussed in Section 3, also manifests itself in ferromagnetic materials with the Rashba spin-orbit coupling [82]. The spin-orbit torques for an antiferromagnetic metal can therefore be expressed as $\mathbf{T}_n^{\mathrm{SOT}} = A\eta\mathbf{n} \times (\hat{\mathbf{z}} \times \mathbf{j})$ and $\mathbf{T}_m^{\mathrm{SOT}} = A\eta\mathbf{m} \times (\hat{\mathbf{z}} \times \mathbf{j})$, where $\eta = J\mathcal{A}\Delta\lambda/(evhw^2)$ and the total magnetization is $\mathbf{m} = (\mathbf{S}_{\mathrm{A}} + \mathbf{S}_{\mathrm{B}})/(2S)$.

In the semimetallic regime ($\varepsilon_F = 0.05w$, see Fig. 7), one of the valleys has only one Fermi surface. Interestingly, the conductivity in this regime is determined by the dependence of the antiferromagnetic order vector on the polar angle: for $n_z^2 < 1/2$, the system is poorly conducting, but the coefficient A is essentially θ-independent and the antidamping spin torques are absent, $B_{\parallel} = B_{\perp} = 0$. A characteristic feature of the semimetallic regime is the significant contribution to the nonequilibrium spin polarization made by terms with dimensionless coefficients A' and C in expression (43), which are the field-like spin torques of higher harmonics.

The numerical results presented in Fig. 7 convincingly demonstrate that the values of the coefficients A and A' are practically insensitive to disorder, while in the nonconducting regime $n_z^2 < 1/2$, the dependence $C(n_z^2)$ is quite conspicuous.

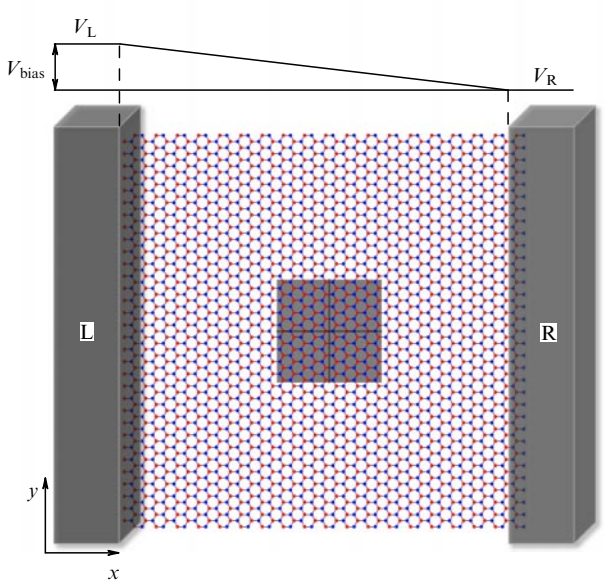

Figure 5. (Color online.) Geometry of a device with two electrodes and a bias V_{bias} between them, which allowed obtaining nonequilibrium spin polarization of conduction electrons [51] within the formalism of scattering matrices [85]. To avoid edge effects, the scattering of conduction electrons is studied in the central region of the setup marked with a gray square.

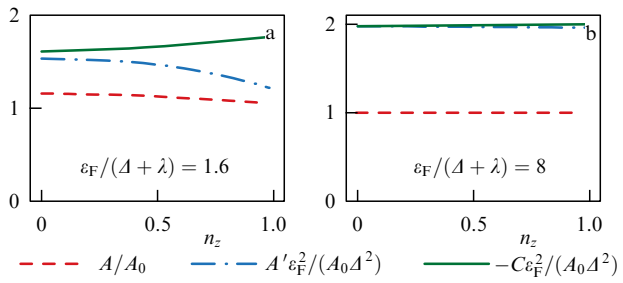

Figure 6. (Color online.) Normalized coefficients A, A', and C depending on the direction of the Néel vector for the metallic regime at (a) $\varepsilon_F = 4\Delta_{sd}$ and (b) $\varepsilon_F = 16\Delta_{sd}$; $A_0 = \Delta_{sd}\mathcal{A}\lambda/(ev\hbar\varepsilon_F S)$.

From the physical standpoint, this dependence on the impurity concentration is determined by the conduction mechanism. It is worth noting that a semimetallic antiferromagnet is not purely speculative: in particular, it has been found in Mn_2Ru_xGa [83, 84].

Before proceeding to the microscopic analysis of Gilbert damping, we briefly discuss the case where the s–d exchange interaction between localized magnetic moments and conduction electron spins is present in only one sublattice,

$$H_{sd} = -J\sum_{i\in A}\sum_{\sigma\sigma'}\mathbf{S}_{iA}\boldsymbol{\sigma}_{\sigma\sigma'}c^{\dagger}_{i\sigma}c_{i\sigma'}\,. \tag{45}$$

Such an interaction breaks the symmetry of the system with respect to the sublattices, which can in turn give rise to the nonequilibrium spin polarization $\delta\mathbf{s}^-$ and hence antidamping spin-orbit torques, which are absent in the symmetric case considered above. We note that the model with an asymmetric exchange interaction is more suitable for describing a ferrimagnet, such as GdFeCo, where conduction electrons mainly interact only with d-localized orbitals [86]. In full analogy with the calculations presented above, the spin-orbit

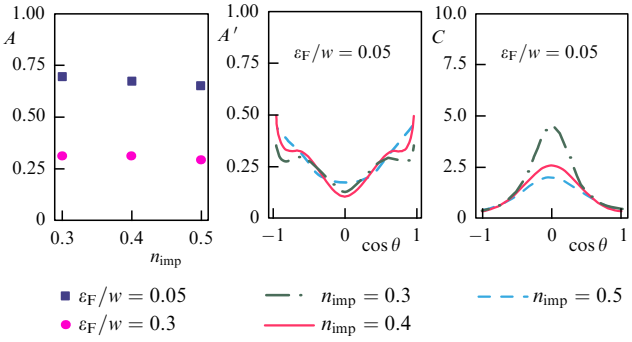

Figure 7. (Color online.) Coefficients determining the expansion of the nonequilibrium spin polarization of conduction electrons $\delta\mathbf{s}^+$ in metallic ($\varepsilon_F/w = 0.3$) and semimetallic ($\varepsilon_F/w = 0.05$) modes depending on impurity concentration n_{imp} corresponding to the amount of impurity, each treated as a local random scalar potential divided by the number of lattice sites.

torque in this system, which acts only on the A-sublattice magnetization $\mathbf{n}_A$, is defined as

$$\begin{aligned}\mathbf{T}^A = \eta\Big[&A(n_z^2)\mathbf{n}_A\times(\hat{\mathbf{z}}\times\mathbf{j}) + B_\perp(n_z^2)\mathbf{n}_A\times\left(\mathbf{n}_A^\perp\times(\hat{\mathbf{z}}\times\mathbf{j})\right)\\ &+ B_\parallel(n_z^2)\mathbf{n}_A\times\left(\mathbf{n}_A^\parallel\times(\hat{\mathbf{z}}\times\mathbf{j})\right)\\ &+ C(n_z^2)\mathbf{n}_A\times\left(\mathbf{n}_A^\parallel\times\left(\mathbf{n}_A^\perp\times(\hat{\mathbf{z}}\times\mathbf{j})\right)\right)\Big]\,,\end{aligned} \tag{46}$$

where the coefficients A, $B_\perp$, $B_\parallel$, and C are nontrivial functions of n_z^2 shown in Fig. 8. In this case, as is easy to understand, the Néel vector coincides with $\mathbf{n}_A$.

In contrast to the symmetric model, note the appearance of antidamping torques with the coefficients $B_\perp$ and $B_\parallel$. We note that their contribution strongly depends on the level of disorder, in contrast to the contributions of the field-like torques, which are mainly determined by the first term in expression (46). We can see from Fig. 8 that, as disorder in the system increases, the antidamping torques disappear in the metallic regime and increase in the semimetallic regime.

To summarize, we note that the experimentally determined contributions from both field-like and antidamping torques in GdFeCo ferrimagnet films with perpendicular magnetocrystalline anisotropy, where the possibility of magnetization switching under the action of spin-orbit torques is of particular interest [87–89], qualitatively coincide with the results obtained within the microscopic approach presented in this section.

4.3 Antiferromagnetic switching

As we have noted, the field-like and antidamping torques affect the antiferromagnetic order vector, which proved the path to study the possibility of the Néel vector switching in the system. For a single-domain antiferromagnet, the magnetic dynamics is determined by the system of Landau–Lifshitz–Gilbert equations for the magnetization vectors of both sublattices, $\mathbf{n}_A$ and $\mathbf{n}_B$:

$$\begin{aligned}\frac{\partial\mathbf{n}_A}{\partial t} &= \frac{J_{ex}S}{2\hbar}\,\mathbf{n}_B\times\mathbf{n}_A + \frac{J_{sd}\mathcal{A}}{\hbar}\,\mathbf{n}_A\times\delta\mathbf{s}_A + \alpha\mathbf{n}_A\times\frac{\partial\mathbf{n}_A}{\partial t}\,,\\ \frac{\partial\mathbf{n}_B}{\partial t} &= \frac{J_{ex}S}{2\hbar}\,\mathbf{n}_A\times\mathbf{n}_B + \frac{J_{sd}\mathcal{A}}{\hbar}\,\mathbf{n}_B\times\delta\mathbf{s}_B + \alpha\mathbf{n}_B\times\frac{\partial\mathbf{n}_B}{\partial t}\,,\end{aligned} \tag{47}$$

where J_{ex} is the antiferromagnetic exchange energy. In Fig. 9, we show the numerical results for the system of equations for

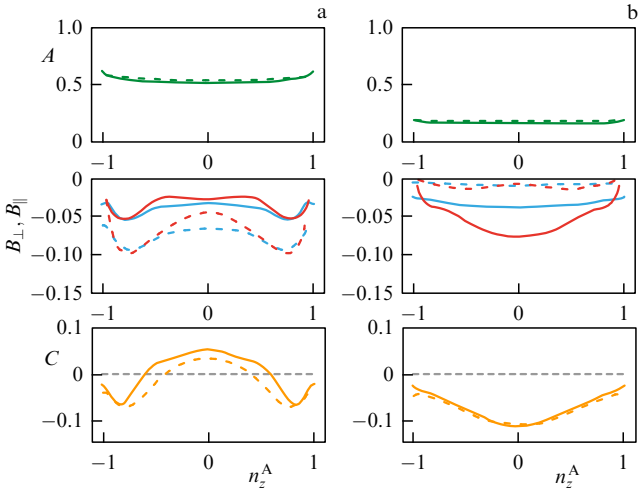

Figure 8. (Color online.) Coefficients A (green curves), $B_\perp$ (blue curves), $B_\parallel$ (red curves), and C (yellow curves) that determine the spin-orbit torque in asymmetric model (45) depending on the orientation of the Néel vector at (a) $\varepsilon_F/w = 0.1$ and (b) $\varepsilon_F/w = 0.3$. Solid curves correspond to $n_{imp} = 0.3$, dashed curves, to $n_{imp} = 0.5$.

the components of the Néel vector under the effect of short current pulses alternating between the directions $-\hat{\mathbf{x}}$ and $\hat{\mathbf{y}}$. As can be seen, in the sublattice-symmetric model, the spin-orbit torques due to the nonequilibrium spin polarization $\delta\mathbf{s}^+$ are not enough to change the orientation of the Néel vector, whereas in the asymmetric model we observe the effect of antiferromagnetic switching determined mainly by field-like torques with the coefficients A and C [51].

4.4 Gilbert damping

Unlike conductivity and spin-orbit torques, which are practically isotropic for the antiferromagnet model with a strong spin-orbit coupling in the metallic regime, Gilbert damping is essentially anisotropic in the Landau–Lifshitz–Gilbert equations

$$\begin{aligned}\dot{\mathbf{n}} &= -\frac{2J_{ex}S}{\hbar}\,\mathbf{n}\times\mathbf{m} + \mathbf{H}\times\mathbf{n} + \alpha_m^{\parallel}\mathbf{n}\times\dot{\mathbf{m}}_{\parallel} + \alpha_n^{\perp}\mathbf{m}\times\dot{\mathbf{n}}_{\perp}\,,\\ \dot{\mathbf{m}} &= \mathbf{H}\times\mathbf{m} + \alpha_n^{\perp}\mathbf{n}\times\dot{\mathbf{n}}_{\perp} + \alpha_m^{\parallel}\mathbf{m}\times\dot{\mathbf{m}}_{\parallel}\,,\end{aligned} \tag{48}$$

where

$$\begin{aligned}\alpha_m^{\parallel} &= \frac{2\varepsilon_F\tau}{\hbar}\,\frac{\mathcal{A}}{\pi S}\left(\frac{\Delta_{sd}}{\hbar v}\right)^2\left[1-\frac{\Delta^2}{\varepsilon_F^2}(2+n_z^2)+\ldots\right],\\ \alpha_n^{\perp} &= \frac{\varepsilon_F\tau}{\hbar}\,\frac{\mathcal{A}}{\pi S}\left(\frac{\Delta_{sd}}{\hbar v}\right)^2\left[\left(\frac{\lambda}{\varepsilon_F}\right)^2+\ldots\right].\end{aligned} \tag{49}$$

The anisotropy of the Gilbert damping in a Rashba antiferromagnet arises due to the splitting of the electron subbands under the influence of the spin-orbit coupling. An interesting consequence of this anisotropy is the presence of an undamped nonequilibrium dynamical mode corresponding to the ultrafast precession of the Néel vector in the antiferromagnet plane. A detailed discussion and calculation details are presented in [52].

5. Conclusion

Studying magnetic dynamics in low-dimensional collinear magnetic systems is a complex problem, whose solution

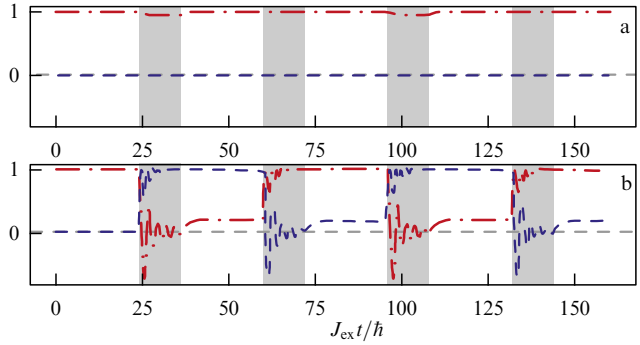

Figure 9. (Color online.) Dynamics of the magnetization vector in the sample plane in the (a) symmetric and (b) asymmetric model under the action of a series of short current pulses alternating between directions $-\hat{\mathbf{x}}$ and $\hat{\mathbf{y}}$ as indicated by the gray areas. Red curves correspond to $n_x(t)$, blue curves, to $n_y(t)$. Solution was obtained using the expressions for $\delta\mathbf{s}_{A,B}$ with $\alpha = 0.1$.

within the phenomenological analysis turns out to be generally insufficient. In this review, we have discussed a microscopic approach to the derivation of spin-orbit and spin-transfer torques, Gilbert damping, and symmetric and asymmetric exchange interaction constants using the models of two-dimensional ferromagnets and antiferromagnets with a strong Rashba spin-orbit coupling within the s–d exchange model.

In particular, for a two-dimensional Rashba ferromagnet, we calculated the Dzyaloshinskii–Moriya interaction constant as a function of temperature in the Rashba–Bychkov model; expressions for spin-orbit and spin-transfer torques were obtained. We have shown that the presence of a strong spin-orbit coupling leads to an orientational anisotropy of the Gilbert damping and spin-transfer torques; we also discussed spin renormalization problems.

For the Rashba model of a two-dimensional antiferromagnet on a hexagonal lattice, we discussed the spin-transfer torques in the metallic and semimetallic regimes both in the presence of the sublattice symmetry corresponding to equal exchange interaction constants for the sublattices as well as in its absence. In the symmetric model, the nonequilibrium spin polarization of conduction electrons is determined by a field-like term, while the antidamping-like contribution is completely absent, but appears when the symmetry with respect to the sublattices is broken. It is especially interesting that the antidamping torques in the asymmetric model are highly anisotropic and exhibit a pronounced dependence on the impurity concentration in both the metallic and semimetallic regimes. The presented results offer a new perspective on the processes occurring in magnetic systems and are important for the analysis of a wide range of experimental studies on switching the magnetic order parameter.

Acknowledgments

The authors express their sincere gratitude to M L Titov and M I Katsnelson for the numerous helpful discussions. The work of A A P was supported by grants from the Russian Science Foundation (project 20-72-00044, Section 3) and the Russian Foundation for Basic Research (RFBR) (project 19-32-60020, Section 4), and a scholarship of the President of the Russian Federation (SP-1640.2021.5, Section 4); the work of D I Yu was supported by the RFBR (project 20-52-S52001).

References

1. Saurenbach F et al. *J. Appl. Phys.* **63** 3473 (1988)
2. Baibich M N et al. *Phys. Rev. Lett.* **61** 2472 (1988)
3. Fert A *Rev. Mod. Phys.* **80** 1517 (2008); *Usp. Fiz. Nauk* **178** 1336 (2008)
4. Grünberg P A *Rev. Mod. Phys* **80** 1531 (2008); *Usp. Fiz. Nauk* **178** 1349 (2008)
5. Slonczewski J C *J. Magn. Magn. Mater.* **159** L1 (1996)
6. Berger L *Phys. Rev. B* **54** 9353 (1996)
7. Sinova J et al. *Rev. Mod. Phys.* **87** 1213 (2015)
8. Pudalov V M *Phys. Usp.* **64** 3 (2021); *Usp. Fiz. Nauk* **191** 3 (2021)
9. Nikitov S A et al. *Phys. Usp.* **58** 1002 (2015); *Usp. Fiz. Nauk* **185** 1099 (2015)
10. Nikitov S A et al. *Phys. Usp.* **63** 945 (2020); *Usp. Fiz. Nauk* **190** 1009 (2020)
11. Fraerman A A *Phys. Usp.* **55** 1255 (2012); *Usp. Fiz. Nauk* **182** 1345 (2012)
12. Pyatakov A P et al. *Phys. Usp.* **58** 981 (2015); *Usp. Fiz. Nauk* **185** 1077 (2015)
13. Borisov A B *Phys. Usp.* **63** 269 (2020); *Usp. Fiz. Nauk* **190** 291 (2020)
14. Žutić I, Fabian J, Das Sarma S *Rev. Mod. Phys.* **76** 323 (2004)
15. Zvezdin A K, Zvezdin K A, Khval'kovskii A V *Phys. Usp.* **51** 412 (2008); *Usp. Fiz. Nauk* **178** 436 (2008)
16. Gulyaev Yu V et al. *Phys. Usp.* **52** 335 (2009); *Usp. Fiz. Nauk* **179** 359 (2009)
17. Baranov P G et al. *Phys. Usp.* **62** 795 (2019); *Usp. Fiz. Nauk* **189** 849 (2019)
18. Zakharchenya B P, Korenev V L *Phys. Usp.* **48** 603 (2005); *Usp. Fiz. Nauk* **175** 629 (2005)
19. Volkov N V *Phys. Usp.* **55** 250 (2012); *Usp. Fiz. Nauk* **182** 263 (2012)
20. Pyatakov A P, Zvezdin A K *Phys. Usp.* **55** 557 (2012); *Usp. Fiz. Nauk* **182** 593 (2012)
21. Zvezdin A K, Davydova M D, Zvezdin K A *Phys. Usp.* **61** 1127 (2018); *Usp. Fiz. Nauk* **188** 1238 (2018)
22. Gomonay E V, Loktev V M *Low Temp. Phys.* **40** 17 (2014); *Fiz. Nizk. Temp.* **40** 22 (2014)
23. Baltz V et al. *Rev. Mod. Phys.* **90** 015005 (2018)
24. Katine J A et al. *Phys. Rev. Lett.* **84** 3149 (2000)
25. Kubota H et al. *Nat. Phys.* **4** 37 (2008)
26. Miron I M et al. *Nature* **476** 189 (2011)
27. Liu L et al. *Science* **336** 555 (2012)
28. Jungwirth T et al. *Nat. Nanotechnol.* **11** 231 (2016)
29. Park B G et al. *Nat. Mater.* **10** 347 (2011)
30. Duine R *Nat. Mater.* **10** 344 (2011)
31. Wadley P et al. *Nat. Commun.* **4** 2322 (2013)
32. Kosub T et al. *Nat. Commun.* **8** 13985 (2017)
33. Olejník K et al. *Nat. Commun.* **8** 15434 (2017)
34. Manchon A et al. *Rev. Mod. Phys.* **91** 035004 (2019)
35. Soumyanarayanan A et al. *Nature* **539** 509 (2016)
36. Pham V T et al. *Nat. Electron.* **3** 309 (2020)
37. Ado I A, Tretiakov O A, Titov M *Phys. Rev. B* **95** 094401 (2017)
38. Ralph D C, Stiles M D *J. Magn. Magn. Mater.* **320** 1190 (2008)
39. van der Bijl E, Duine R A *Phys. Rev. B* **86** 094406 (2012)
40. Hals K M D, Brataas A *Phys. Rev. B* **88** 085423 (2013)
41. Garello K et al. *Nat. Nanotechnol.* **8** 587 (2013)
42. Qaiumzadeh A, Duine R A, Titov M *Phys. Rev. B* **92** 014402 (2015)
43. Koumpouras K, Bergman A, Eriksson O, Yudin D *Sci. Rep.* **6** 25685 (2016)
44. Yudin D, Gulevich D R, Titov M *Phys. Rev. Lett.* **119** 147202 (2017)
45. Qaiumzadeh A et al. *Phys. Rev. Lett.* **120** 197202 (2018)
46. Ado I A et al. *Phys. Rev. Lett.* **121** 086802 (2018)
47. Koumpouras K et al. *J. Phys. Condens. Matter* **30** 375801 (2018)
48. Pervishko A A et al. *Sci. Rep.* **8** 17148 (2018)
49. Bessarab P F et al. *Phys. Rev. B* **99** 140411 (2019)
50. Sokolewicz R J et al. *Phys. Rev. B* **99** 214444 (2019)
51. Sokolewicz R J et al. *Phys. Rev. B* **100** 214403 (2019)
52. Baglai M et al. *Phys. Rev. B* **101** 104403 (2020)
53. Ado I A et al. *Phys. Rev. B* **101** 161403 (2020)
54. Ado I A, Ostrovsky P M, Titov M *Phys. Rev. B* **101** 085405 (2020)
55. Pervishko A A et al. *Opt. Express* **28** 29155 (2020)
56. Streda P *J. Phys. C* **15** L717 (1982)
57. Sinitsyn N A et al. *Phys. Rev. B* **75** 045315 (2007)
58. Dzyaloshinsky I *J. Phys. Chem. Solids* **4** 241 (1958)
59. Moriya T *Phys. Rev.* **120** 91 (1960)
60. Ado I A et al. *Europhys. Lett.* **111** 37004 (2015)
61. Ado I A et al. *Phys. Rev. Lett.* **117** 046601 (2016)
62. Edelstein V M *Solid State Commun.* **73** 233 (1990)
63. Edelstein V M *Phys. Rev. Lett.* **80** 5766 (1998)
64. Inoue J, Bauer G E W, Molenkamp L W *Phys. Rev. B* **67** 033104 (2003)
65. Železný J et al. *Phys. Rev. Lett.* **113** 157201 (2014)
66. Wadley P et al. *Science* **351** 587 (2016)
67. Fina I, Marti X *IEEE Trans. Magn.* **53** 2500107 (2017)
68. Saidl V et al. *Nat. Photon.* **11** 91 (2017)
69. Železný J et al. *Nat. Phys.* **14** 220 (2018)
70. Barthem V M T S et al. *Nat. Commun.* **4** 2892 (2013)
71. Jourdan M et al. *J. Phys. D* **48** 385001 (2015)
72. Bhattacharjee N et al. *Phys. Rev. Lett.* **120** 237201 (2018)
73. Pandey S K, Mahadevan P, Sarma D D *Europhys. Lett.* **117** 57003 (2017)
74. Tshitoyan V et al. *Phys. Rev. B* **92** 214406 (2015)
75. Železný J et al. *Phys. Rev. B* **95** 014403 (2017)
76. Manchon A *J. Phys. Condens. Matter* **29** 104002 (2017)
77. Ghosh S, Manchon A *Phys. Rev. B* **98** 220412 (2018)
78. Watanabe H, Yanase Y *Phys. Rev. B* **98** 220412 (2018)
79. Kane C L, Mele E J *Phys. Rev. Lett.* **95** 146802 (2005)
80. Qiao Z et al. *Phys. Rev. B* **85** 115439 (2012)
81. Šmejkal L et al. *Phys. Rev. Lett.* **118** 106402 (2017)
82. Garate I, MacDonald A H *Phys. Rev. B* **80** 134403 (2009)
83. Kurt H et al. *Phys. Rev. Lett.* **112** 027201 (2014)
84. Betto D et al. *AIP Adv.* **6** 055601 (2016)
85. Lesovik G B, Sadovskyy I A *Phys. Usp.* **54** 1007 (2011); *Usp. Fiz. Nauk* **181** 1041 (2011)
86. Jungfleisch M B, Zhang W, Hoffmann A *Phys. Lett. A* **382** 865 (2018)
87. Kim J et al *Sci. Rep.* **8** 6017 (2018)
88. Roschewsky N et al. *Appl. Phys. Lett.* **109** 112403 (2016)
89. Roschewsky N, Lambert C-H, Salahuddin S *Phys. Rev. B* **96** 064406 (2017)